Proceedings of ASME Turbo Expo 2021
Turbomachinery Technical Conference and Exposition
GT2021
June 7-11, 2021, Virtual, Online

GT2021-58618

NUMERICAL CALIBRATION AND INVESTIGATION OF THE INFLUENCE OF REYNOLDS NUMBER ON MEASUREMENTS WITH FIVE-HOLE PROBES IN COMPRESSIBLE FLOWS

Christian Schäffer, Konstantin Speck, Volker Gümmer
Chair of Turbomachinery and Flight Propulsion
Department of Aerospace and Geodesy
Technical University of Munich
Boltzmannstr. 15, 85748 Garching, Germany
Email: christian.schaeffer@tum.de

ABSTRACT

This paper presents an investigation into the numerical and experimental calibration of a five-hole probe and effects of Reynolds number variations on the characteristics of the probe. The test object is a cone-type drilled elbow probe with a head diameter of 1.59 mm and a cone angle of $60°$*. The experimental calibration maps of four different probes of the same type and nominal geometry are compared. A significant variation of the curves can be observed especially at high yaw angles. This led to a visual inspection of the probes with a 3D measurement system. The actual geometry of the three used probes and the surface and radii in particular varied significantly from that of the unused spare probe.*

Furthermore, a numerical calibration map of the ideal probe was generated for a Mach number of $Ma = 0.3$*. A comparison between the experimental and numerical calibration coefficients revealed that total pressure, yaw and pitch angle were reproduced reasonably well. The dynamic pressure coefficient, however, has a considerable offset.*

Finally, a parameter study of the effect of varying the Reynolds number over different yaw angles was conducted. The calibration Reynolds number is of the order of $Re = 1 \cdot 10^4$ *and was varied between* $0.5 \cdot 10^4 < Re < 6 \cdot 10^4$*. While the results suggest that only minor measurement errors occur for yaw angle, total pressure and static pressure, a relatively large error was observed for pitch angle measurements.*

KEYWORDS

Five-hole probe, Numerical calibration, Ansys Fluent

INTRODUCTION

The detailed understanding of flow phenomena in turbomachinery remains an ongoing challenge. Probes with high spatial resolution are required to accurately resolve the flow within modern high-speed compressors or turbines. Pneumatic multi-hole probes are widely used to measure pressures, angles and - in combination with temperatures - velocity components in turbomachinery. These probes are usually calibrated in wind tunnels at different Mach numbers, but typically under uniform, steady flow conditions with low turbulence levels and ambient pressures. However, in high-speed turbomachinery applications, the probes are subject to highly unsteady flows with strong shear gradients, high turbulence levels and quite often also to significantly different Reynolds numbers due to operating pressures greater than the ambient pressure. All of these can have non-negligible influences on the calibration characteristics of the probes, and thus on the measured flow properties.

In this study, a numerical model is developed for a commercially-supplied five-hole probe in order to carry out systematic investigations under controlled conditions on the effects of Reynolds number variations on the calibration characteristic of the probe.

A detailed 3D-flow analysis for a multi-hole pressure probe was conducted by de Guzman et al. [1] in incompressible flows at low Reynolds numbers ($Re = 2 \cdot 10^3$) using RANSTAD with the k-epsilon turbulence model. The numerical calibration showed good quantitative agreement with the experimental results.

Coldrick et al. [2] carried out a general investigation of the measurement uncertainties of five-hole probes in compressor flows by means of steady and unsteady flow simulations. For this purpose, a numerical calibration map was generated to investigate the blockage effect of multi-hole probes in compressor applications. One main finding was that a steady state disturbance can cause errors in the probe measurements while effects from the unsteadiness produced by a compressor have a negligible effect on the probe characteristics.

A numerical calibration map for a five-hole probe was generated by Aschenbruck et al. [3] using the SST turbulence model of Ansys CFX. A comparison between the experimental and numerical calibration identified good agreement for the total pressure and yaw coefficient for different yaw angles. In contrast, the static pressure and pitch coefficients exhibited a significant deviation. Aschenbruck et al. [3] hypothesized that the source of the error, especially for high yaw incidence, might originate from the difference in shape between the actual geometry of the probe head and the geometry used for the numerical calibration.

Passmann et al. [4] introduced a procedure for calibrating additively manufactured multi-hole probes based on 3D scanning followed by a numerical calibration with the actual scanned geometry. Therefore, a compressible, steady-state RANS solver was utilized which provided predictions for a numerical calibration map in subsonic flows within a yaw and pitch angle error of 2.5° and a total pressure deviation of less than 1.5%.

However, the most recent investigations from Coldrick et al. [2], Aschenbruck et al. [3], Passmann et al. [4], Sanders et al. [5] and Arguelles Diaz et al. [6] did not consider the geometry of the probe holes and modeled only the probe surface in their investigations. In contrast, LI et al. [7] stated that modeling of the actual probe hole geometry is significant if accurate numerical results are to be achieved.

Dominy et al. [8] considered the effect of Reynolds number variation on the calibration of five-hole probes, identifying a major effect at low Reynolds numbers. The flow separation at the probe head under incidence results in sensitivity changes in the yaw measurement.

Arguelles Diaz et al. [6] investigated the effect of small Reynolds number changes in the range $Re = 1 \cdot 10^4$ to $Re = 2.4 \cdot 10^4$ using a one-equation turbulence model. The numerical and experimental calibration generally agree well, however, at large yaw angles the numerical model did not accurately reproduce the effect of Reynolds number changes when compared to the experimental calibration.

A numerical study of the influence of Reynolds number on calibration maps was also carried out by LI et al. [7]. Effects due to modeling of the probe holes are presented and stated to be significant for numerical investigations of multi-hole probes. The study was conducted for $Ma = 0.35$ at $5.25 \cdot 10^4 < Re < 2.63 \cdot 10^5$ and reference pressures below ambient of 0.0709 MPa and 0.5065 MPa while varying the yaw angle up to 20°. The results show a significant deviation in the pressure coefficients if the Reynolds number of the calibration differs significantly from that of the measurement.

An experimental study investigating the effect of Reynolds number variation in the range of $6.60 \cdot 10^3 < Re < 3.17 \cdot 10^4$ over a yaw and pitch angle range of $-35^\circ < \alpha, \beta < 35^\circ$ was conducted by Lee et al. [9]. It was shown that deviations in the Reynolds number between calibration and measurements lead to appreciable measurement errors. A significant error in the total pressure coefficient occurs at incidences greater than 20°. Furthermore, the static pressure coefficient tends to be sensitive over almost the whole incidence range.

Passmann et al. [10] also carried out an experimental investigation of the Reynolds number effect on five-hole probe performance. Their study gives a deeper insight into the Re sensitivity mechanisms with the help of PIV techniques and oil flow visualizations.

The present study focuses on setting up a numerical model that is able to reproduce the experimental calibration data in a reasonable manner, while taking into account the effect of modeling the probe holes. To do so, four actual five-hole probe calibrations of probes with the same nominal geometry are analyzed and compared to the results of a numerical calibration. Since five-hole probes are often used in areas with higher pressure levels but calibrated at ambient pressure, this investigation also concentrates on measurement uncertainties in flow conditions with higher density at constant Mach number, hence for higher Reynolds numbers.

The five-hole probes considered in this study are eccentric ferrule probes. This is a drilled elbow probe made from stainless steel with a cone angle of 60°. Figure 1 shows the arrangement of the probe holes and the nominal dimensions of the probe head.

The probes are used in the High Speed Research Compressor (HSRC) at TUM. As the compressor has 3.5 stages with three circumferentially distributed slots behind each rotor and stator, use of three of the available probes allows measuring downstream of all rotors or stators at the same time. An additional fourth probe functions as spare. All four probes are considered in the following investigations. The experimental calibration describes the characteristics of the four real probes, while the numerical calibration represents the actual numerical results of the ideal probe.

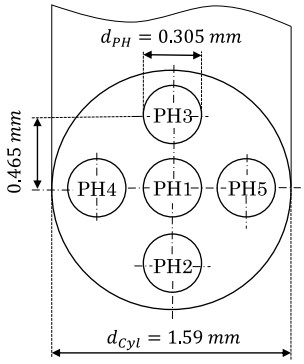

FIGURE 1. FRONTAL VIEW - DIMENSIONS AND PROBE HOLE NOMENCLATURE

CALIBRATION PROCEDURE

The probes are rotated in yaw direction α (cf. Fig. 3) during traversing in the test rig to maintain relative flow angles close to 0°. The real probes are calibrated over a yaw angle range of $-30° < \alpha < 30°$. The expected pitch angle tends also to be within $-30° < \beta < 30°$. Probe calibration was carried out in a low-turbulence calibration channel over a Mach number range of $0.1 < Ma < 0.64$. This results in four different non-dimensional calibration coefficients for each Mach number, each over a two-dimensional grid with yaw (α) and pitch (β) angles as the coordinates (cf. Fig. 2). A familiar definition of the calibration coefficients is given by Treaster et al. [11]. However, in the present study the coefficients are defined as follows:

$$C_{yaw} = \frac{P_{PH5} - P_{PH4}}{P_{max} - P_{avg}} \tag{1}$$

$$C_{pitch} = \frac{P_{PH3} - P_{PH2}}{P_{max} - P_{avg}} \tag{2}$$

$$C_{P_t} = \frac{P_t - P_{PH1}}{P_{max} - P_{avg}} \tag{3}$$

$$C_{P_d} = \frac{P_t}{P_{max} - P_{avg}} \tag{4}$$

$$P_{max} = \frac{P_{PH1} + max(P_{PH1-PH5})}{2} \tag{5}$$

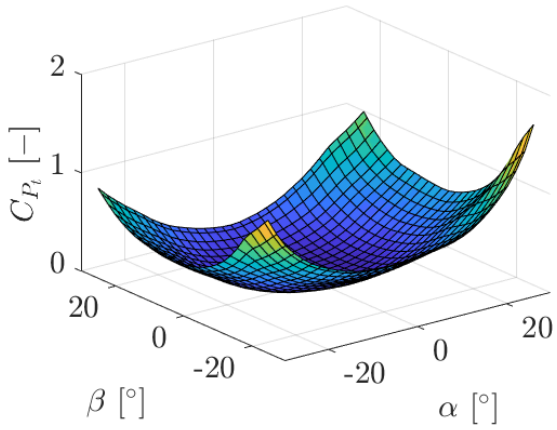

FIGURE 2. TOTAL PRESSURE COEFFICIENT FOR EXPERIMENTAL CALIBRATION AT $Ma = 0.3$

$$P_{avg} = \frac{P_{PH2} + P_{PH3} + P_{PH4} + P_{PH5}}{4} \tag{6}$$

The total pressure P_t represents the pressure in the settling chamber of the calibration channel. In the subsequent numerical study, the probe was numerically calibrated over a yaw angle range of $-10° < \alpha < 30°$, a pitch angle range of $-5° < \beta < 5°$ and at a Mach number of $Ma = 0.3$, as the main focus of interest was the behavior at different yaw angles. The accuracy of the used 5 psi-module lies in the range of ±0.05% of full scale, which corresponds to an error of $\varepsilon = \pm 17.5\,Pa$. An error propagation analysis with the maximum possible error of ΔZ resulting from the measurement accuracy of the pressure modules is considered in the representation of the calibration coefficients and marked with error bars in the following figures. The expected value $\overline{Z}$ is calculated from the measured probe hole pressures and total pressure depending on the calibration coefficient (cf. Eq. 1 - 4):

$$\overline{Z} = f(\overline{PH}, \overline{P_t}) \tag{7}$$

Vector Z contains the different combinations of the expected values with the error ε due to the error propagation over the calibration coefficients:

$$Z = f(\overline{PH} \pm \varepsilon, \overline{P_t} \pm \varepsilon) \tag{8}$$

Finally, the error bar represents the maximum difference between the error containing value and the expected value:

$$\Delta Z = max(Z - \overline{Z}) \tag{9}$$

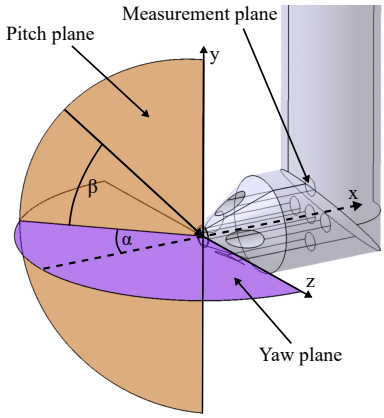

FIGURE 3. LOCATION OF NUMERICAL MEASUREMENT PLANES AND PROBE'S COORDINATE SYSTEM

NUMERICAL SETUP

The numerical model was developed using Fluent Meshing and computed with Ansys Fluent 2020 R1. The simulations were conducted on a workstation equipped with 16 physical cores. As remeshing is necessary for every new angle, the computational time was around 2 hours per angle including meshing. In order to reproduce the probe's behavior in the best possible manner, a full 3D model of the probe was developed based on the nominal shape and dimensions of the probe. This includes the stem and the head with five holes, at the bottom of which the pressures are extracted (cf. Fig. 3, 'Measurement plane') based on the area-weighted average of the total pressure.

Domain

The computational domain is illustrated in Fig. 4. The domain is represented by a 200 mm cube which corresponds to 126 times the head diameter. Based on recommendations from Ansys and in order to minimize interaction with the domain boundaries, the domain was greatly enlarged compared to Willinger et al. [12].

The upstream effect of the probe was estimated using potential theory and verified by CFD in order to minimize any upstream influence of the probe on the boundary conditions at the inlet. To model the flow around a cylinder, the cylindrical stem can be considered as a dipole comprising a source and a sink. Figure 5 shows the change in velocity along the x-axis near the probe for $Ma = 0.3$ and $R = 0.795mm$. Since potential theory does not consider friction forces, the upstream effect is somewhat smaller than that computed using CFD. Based on these results, it can be concluded that the influence of the probe on the domain inlet is negligible because the velocity falls below $\frac{Ma}{Ma_\infty} < 99.9\%$ only 25.14 mm upstream of the center line of the cylinder.

The different yaw and pitch angles were simulated by rotating the probe in an otherwise fixed domain with constant boundary conditions. This approach, which was deemed more practical for the present purpose which includes rather large angle variations and possibly also controlled shear flow and turbulence variations, requires a unique mesh for every angle setting. Finally, the probe tip was positioned in the center of the cube and the probe was rotated around this central point. Table 1 summarizes the domain planes with the respective boundary conditions.

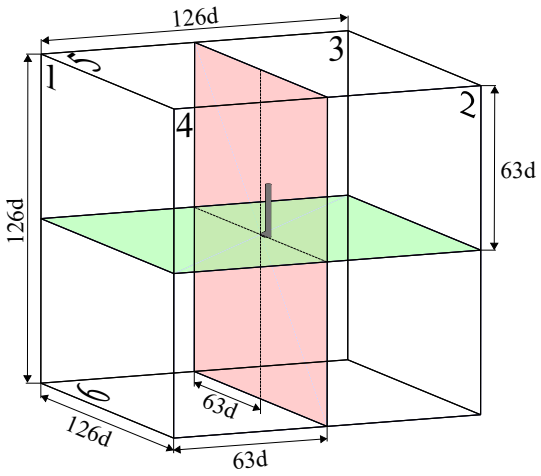

FIGURE 4. DOMAIN SIZE AND LOCATION OF BOUNDARIES IN ACCORDANCE WITH TABLE 1

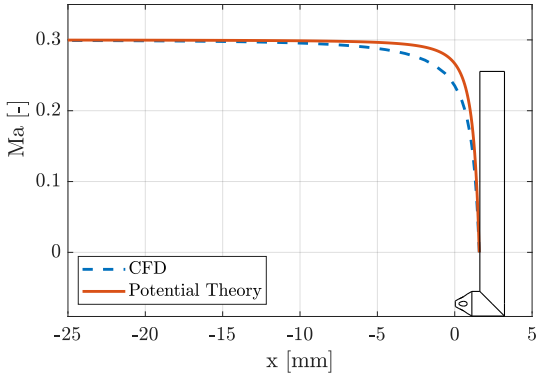

FIGURE 5. UPSTREAM EFFECT CALCULATED USING POTENTIAL THEORY AND CFD

Probe Geometry

The original CAD geometry represents the nominal shape of the real probes. Figure 6 illustrates the deceleration of the velocity along the center line of every probe hole PH1-PH5 at $\alpha = 0°$. Since the probe tip is located at 0 mm, deceleration occurs first at PH1. The side holes PH4 and PH5 are laying on top of each other due to the symmetry of the probe in the x-y plane. The influence of the stem is visible for the top hole PH3 over the first

TABLE 1. BOUNDARY CONDITIONS

PLANE	BOUNDARY CONDITION
1	Velocity inlet $v = 104\,\frac{m}{s}$, $T_t = 300\,K$ Flow direction: Normal to inlet Fluid: Air Density: Compressible, Ideal gas Turbulent Intensity: 1% Turbulent Viscosity Ratio: 10 $\frac{kg}{ms}$
2	Pressure outlet $P_s = 99432\,Pa$, $T_t = 300\,K$
3, 4, 5, 6	Free slip wall
Probe Surface	No slip wall

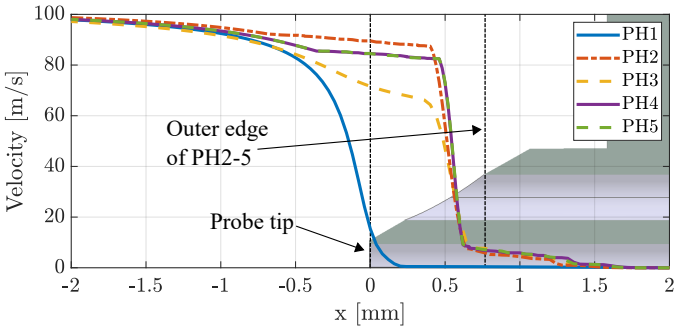

FIGURE 6. VELOCITY DEVELOPMENT INSIDE PROBE HOLES FOR $\alpha = 0°$

0.5 mm. Due to a recirculation area at the side holes a velocity of small magnitude is still present after the 'Outer edge of PH2-5', but disappears before reaching the measurement plane at 2 mm. This is valid for all tested yaw angles α. At the bottom of every probe hole, at the 2 mm location, the kinematic part is completely converted, which means the static pressure equals the total pressure. At this point, the numerical pressure is acquired and averaged over the surface. In the real probes the pressure sensor is actually much further away, namely outside the probe after approximately 10 m of tubing. However, according to Fig. 6, a minimum hole depth to diameter ratio of $\frac{s_{PH2-5}}{d_{PH}} = 4.1$ for the probe holes proved adequate for the numerical model.

Since the probe head has a relatively small overhang of $s_{Tip-Stem} = 1.59\,mm$, the influence of the stem is visible in the measurement of PH3 and under certain yaw angles also at PH4 or PH5. Figure 7 illustrates the total pressure distribution over the surface of the probe head at a yaw angle of $\alpha = 20°$ and a pitch angle of $\beta = 0°$. The potential effect of the stem is clearly visible in the non-symmetrical pressure distribution over the probe head.

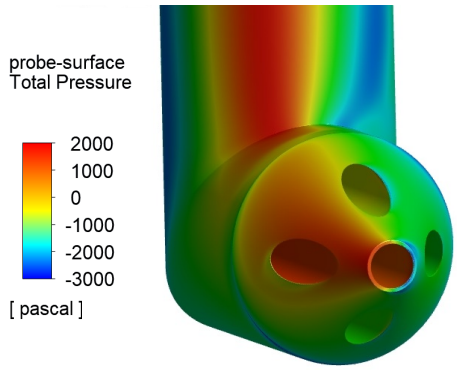

FIGURE 7. TOTAL PRESSURE CONTOUR ON 5HP SURFACE AT $\alpha = 20°$

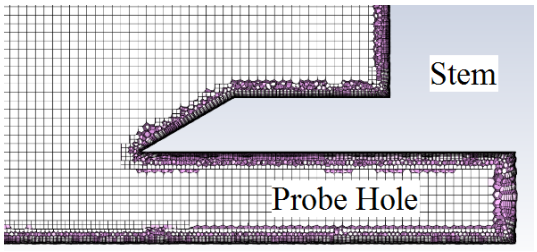

FIGURE 8. MESH DESIGN WITHIN PROBE HOLE 3

Mesh

Due to the complex geometry, Mosaic Meshing Technology with the Poly-Hexcore feature provides a suitable solution for matching different types of meshes [13]. This meshing technology offers a number of advantages, especially where modeling of the probe holes is concerned. A layered polyprism mesh in the boundary layer is connected with general polyhedral elements to the octree hexes in the bulk region (cf. Fig. 8 and Fig. 9). The 10 prism-layers on the probe's surface yielded a $y^+ < 1$ for all presently performed calculations.

A mesh study was conducted to analyze the appropriate mesh density. Three different grids were tested in this investigation. For each case, the local mesh density within the domain is increased progressively towards the probe surface. This yields a coarse grid in the outer region near the domain boundaries and an increasingly finer mesh towards the probe. Table 2 summarizes the main parameters.

Since the probe is symmetric in the x-y plane (cf. Fig. 3) the mesh study was mainly conducted in the positive yaw direction $0° < \alpha < 20°$ at a Mach number of $Ma = 0.30$. A few points were also calculated at negative yaw angles to verify the symmetry of the grids. At PH1 (cf. Fig. 10, top) the sensitivity to grid

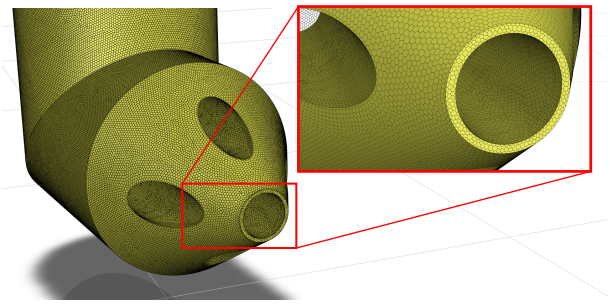

FIGURE 9. POLY-HEXCORE MESH ON PROBE SURFACE

TABLE 2. MESH STUDY PARAMETERS

MESH	NO CELLS	y^+	NO LAYERS
coarse	0.4 Mio.	< 1	10
medium	3.0 Mio.	< 1	10
fine	9.4 Mio.	< 1	10

resolution is mainly visible at yaw angles $-12° > \alpha > 12°$. For the fine mesh, a few additional points were taken in the vicinity of 0°. The differences for this mesh across the symmetry plane are around $\Delta P = 20\,Pa$. Figure 10 (bottom) shows the pressure at PH3. The variation of the pressures between the grids is significantly larger and the symmetrical variation also increases to around $\Delta P = 60\,Pa$ for PH2 and PH3. Overall, the coarse mesh exhibits significant differences in comparison with the medium and fine mesh while the medium and fine mesh are in close agreement. However, the fine mesh was chosen for the following investigations, even though the medium mesh tends to achieve reasonable results and does not differ much from the fine mesh. The choice was made to allow for future studies with significant shear flows and turbulence which are expected to require a finer mesh.

Turbulence Model

The generalized k-omega (GEKO) two-equation turbulence model was used to simulate the probe calibration and to investigate its behavior under different Reynolds number conditions [14]. Arguelles Diaz et al. [6] also applied the one-equation Spalat Almaras model and achieved better results but only for high angles of attack compared to the k-omega model. The GEKO model was chosen because of the planned follow-up studies, which will require a higher-order model.

Convergence

At higher Reynolds numbers, the total pressure inside PH3 tended to oscillate around a constant value over the last iterations. It is likely that these oscillations are provoked by the in-

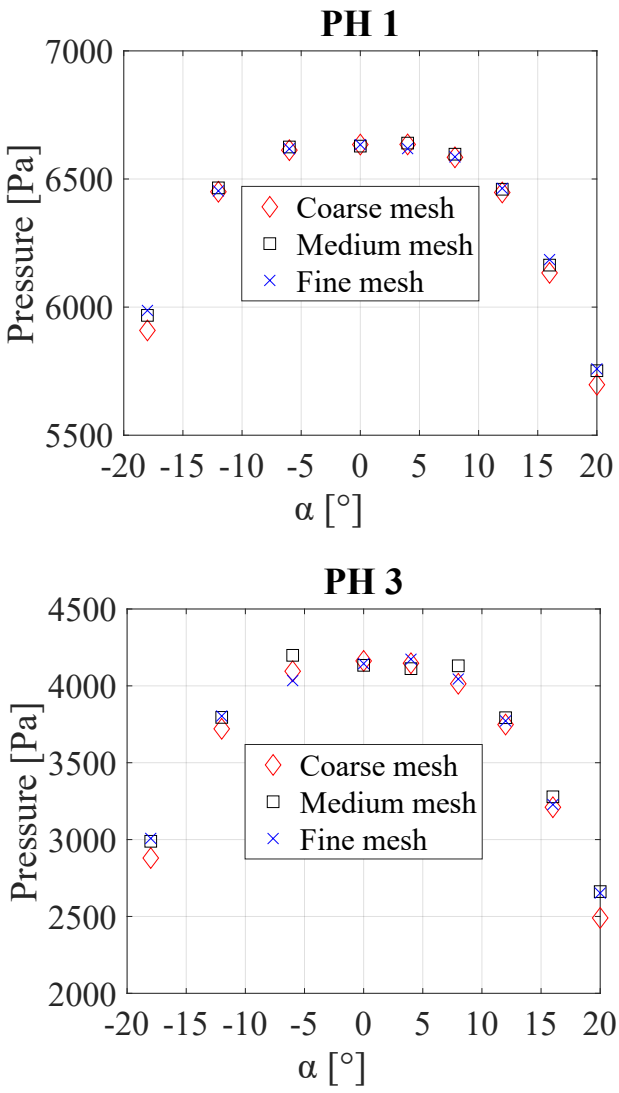

FIGURE 10. YAW ANGLE CALIBRATION WITH THREE DIFFERENT GRIDS, TOP: PRESSURE AT PROBE HOLE 1, BOTTOM: PRESSURE AT PROBE HOLE 3

herently unsteady flow conditions associated with vortex shedding from the stem of the probe. This fact questions the validity of the steady-state computation because the situation favors an unsteady simulation. To assess this factor, an unsteady reference simulation was conducted to quantify the effect of unsteadiness. It was found that the average of the last iterations of the steady simulations agreed well with the unsteady solution. Since the frequency of the oscillation varies for every incidence, a moving average was used to flatten the pressure oscillations. The convergence and averaging criteria were set such that each of the five pressures had to be converged to within the target accuracy corresponding to the experimental measurement system of $\pm 17.5\,Pa$.

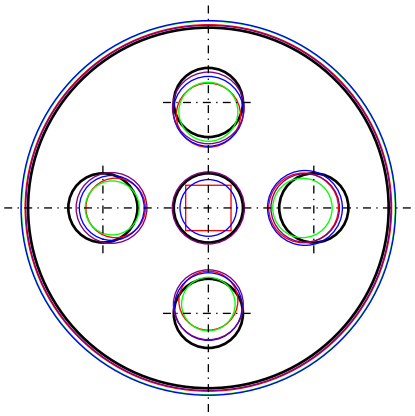

FIGURE 11. REAL PROBE HEAD GEOMETRY - FRONTAL VIEW, BLACK: NOMINAL - RED: PROBE 1 - GREEN: PROBE 2 BLUE: PROBE 3 - VIOLET: PROBE 4

RESULTS

Firstly, a comparison between the initial experimental calibration of all four real probes - calibrated before their extensive use - and the numerical calibration is made in order to investigate the influence of the geometry on the calibration coefficients and to validate the numerical model. Secondly, the influence of modeling the probe holes is shown. Thirdly, a wide-area 3D measurement system from *Keyence* with an accuracy of $\pm 2\,\mu m$ was used to compare the actual probe head geometries with their nominal shape and the results are shown here. Finally, the effect of Reynolds number on the numerical measurement data is assessed.

Numerical and Experimental Calibration

The comparison between the experimental and the numerical calibration for $Ma = 0.3$ and $Re \approx 1.1 \cdot 10^4$ reveals significant deviations in certain areas of the calibration. It is clearly apparent that even amongst the four probes themselves, there is a significant difference in the experimental calibration coefficients. Figure 11 illustrates the deviations of the location and diameter of the probe holes and the probe head itself relative to the nominal geometry. The measurements revealed that the shape of probe 4 (spare probe) comes closest to the nominal geometry. Therefore this probe is highlighted separately in the following figures. The already mentioned error propagation for the experimental calibration is indicated by error bars. The probe spread covers the complete area over which the four probes are extended to emphasize the variation of the real probes that are supposed to have the same nominal geometry. The numerical simulations were performed for this nominal geometry.

Figure 12 presents the total pressure coefficient C_{P_t} over the yaw angle calibration. Within a range of $-4° < \alpha < 4°$ PH1 is quite insensitive to yaw angle changes. However, the further the

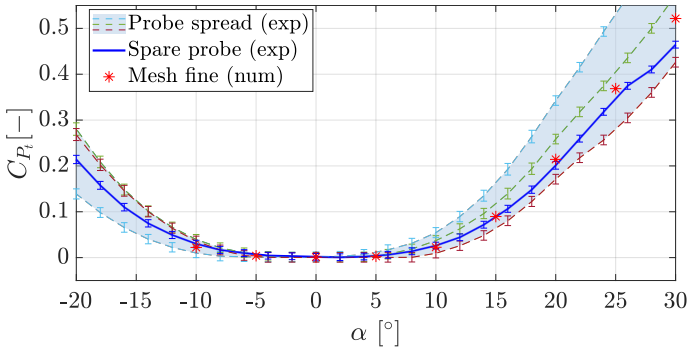

FIGURE 12. TOTAL PRESSURE COEFFICIENT OF EXPERIMENTAL AND NUMERICAL CALIBRATION

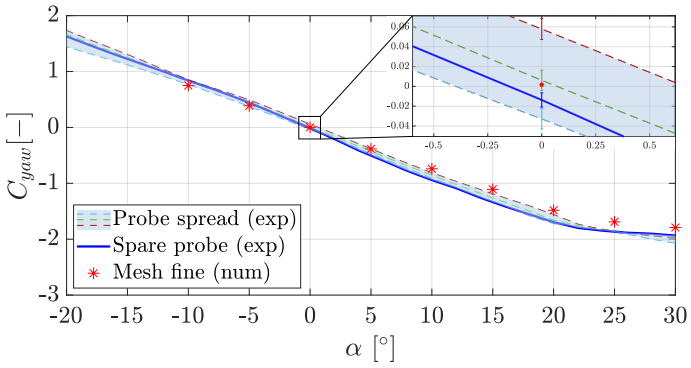

FIGURE 13. YAW ANGLE COEFFICIENT OF EXPERIMENTAL AND NUMERICAL CALIBRATION

probe is rotated away from the center, the larger is the spread in the experimental calibration coefficients of the real probes. The numerical C_{P_t} falls fully within the range of the experimental coefficients and is well aligned with the spare probe.

The experimental yaw angle coefficient C_{yaw} also indicates a progressively larger deviation from the mean value at higher angles (cf. Fig. 13). The numerical calibration points are in good agreement with the experimental points for angles $-10° < \alpha < 10°$. They are slightly outside the range at large angles, as was also observed by Arguelles Diaz et al. [6].

The experimental pitch angle coefficient C_{pitch} is found to vary significantly between the four real probes (cf. Fig. 14). The numerical calibration largely falls within the range.

The spread of the experimental dynamic pressure coefficient C_{P_d} behaves similarly to the total pressure coefficient C_{P_t} for probes 1, 2 and 3 (cf. Fig. 15). At small angles the variation across the three probes is approximately $\Delta C_{P_d} = 0.05$. However, the numerical calibration shows a general offset of around $\frac{C_{P_{d,exp}} - C_{P_{d,num}}}{C_{P_{d,exp}}} = 9\%$. Aschenbruck et al. [3] also observed a significant error in the dynamic pressure coefficient. This deviation might be related to the exact position, size and shape of the pres-

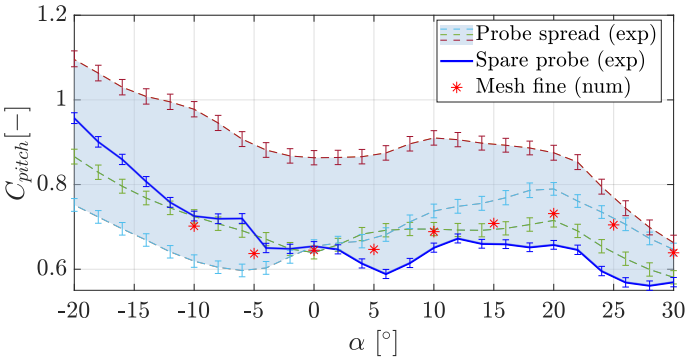

FIGURE 14. PITCH ANGLE COEFFICIENT OF EXPERIMENTAL AND NUMERICAL CALIBRATION

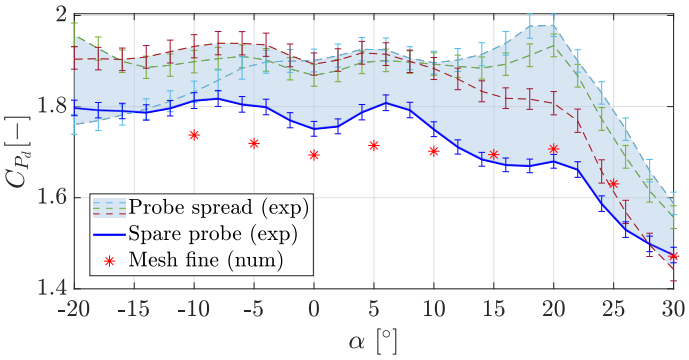

FIGURE 15. DYNAMIC PRESSURE COEFFICIENT OF EXPERIMENTAL AND NUMERICAL CALIBRATION

sure holes because the coefficients and the geometrical shape of the spare probe lie significantly closer to the numerical points and nominal geometry. Therefore, the real probe geometries were found to have some non-negligible deviations from the nominal shape, which was the basis used for the numerical model. This will be discussed later on in the section about real probe geometries. But this issue is also related to the topic of modeling the probe holes.

Modeling Probe Holes

The need for modeling of the probe holes is clearly apparent from Fig. 16, which compares the numerically measured pressures at PH1 and PH4 with and without modeling of the holes. Without the holes modeled, the measured total pressure does indeed behave in a way that is qualitatively similar to the results obtained with probe holes, but is significantly lower for all probe holes. A further analysis of the pressure distribution on the surface where the pressure is measured reveals that, without probe hole modeling, the stagnation point does not cover the entire surface (cf. Fig. 17). This is why the averaging tends to capture lower values. In contrast, modeling of the probe hole leads to

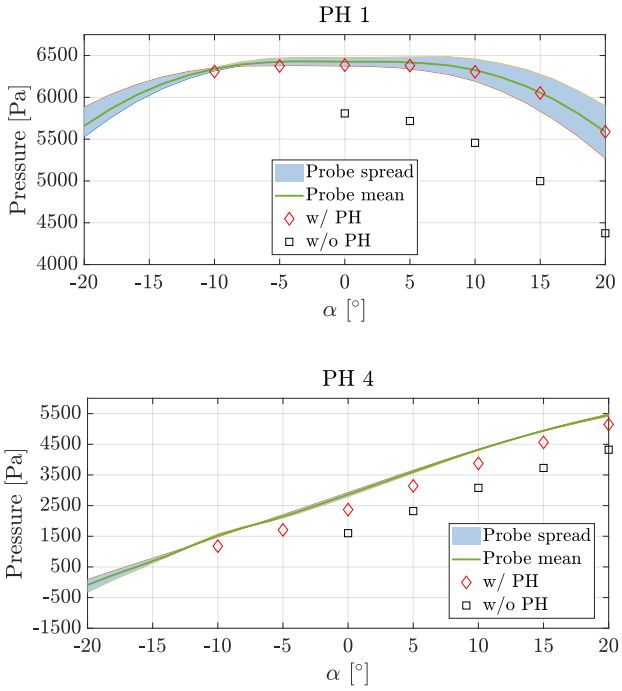

FIGURE 16. PRESSURE MEASUREMENT OF PROBE HOLES W/ AND W/O MODELING THE HOLES

streamlines to the measuring surface at the bottom of the hole where the total pressure is constant over the whole plane. The influence of modeling without probe holes on the calibration coefficient is found to be non-negligible. For yaw angles $\alpha > 10°$ the error in yaw angle measurement increases by up to 2.5°. The pitch angle error lies in the range of 1° without probe holes. The total and static pressure are underestimated by around 1%.

Real Probe Geometry

In order to verify how closely the real probe geometries, used in the present study, correspond to the nominal shape, used in the numerical model, a wide-area 3D measurement system from *Keyence* with an accuracy of $\pm 2\,\mu m$ was utilized to scan the actual probe heads. It should be noted that the resultant deviations can be due either to original manufacturing deviations or aging associated with a few hundred hours of testing in a high-speed compressor environment.

Figure 18 compares two probe heads: one corresponding to a new, unused spare probe and the other to one of the used probes (5HP-1) that has undergone around 300 hours of testing. The center hole in particular exhibits clear signs of abrasion and deformation. The reflective surface around the center hole of the used probe is larger than that of the new one which suggests a flattening of the probe tip. Therefore, significant deviations in the calibration characteristics might be expected, especially at

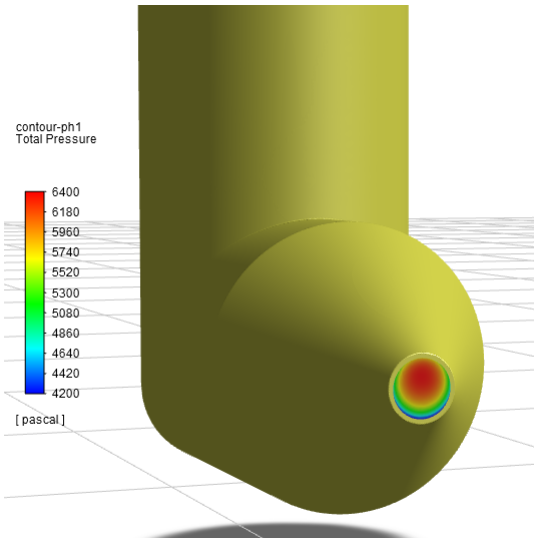

FIGURE 17. AVERAGING SURFACE OF PROBE W/O MODELED PROBE HOLES

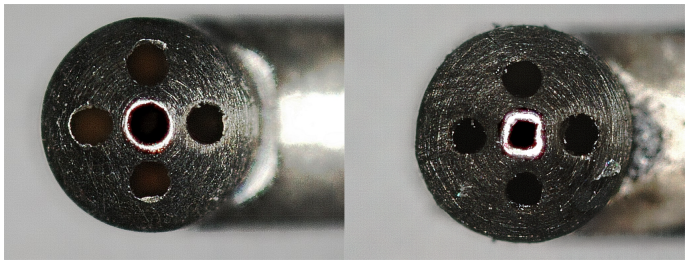

FIGURE 18. LEFT: UNUSED SPARE 5HP-4, RIGHT: 5HP-1 AFTER 300 TESTING HOURS

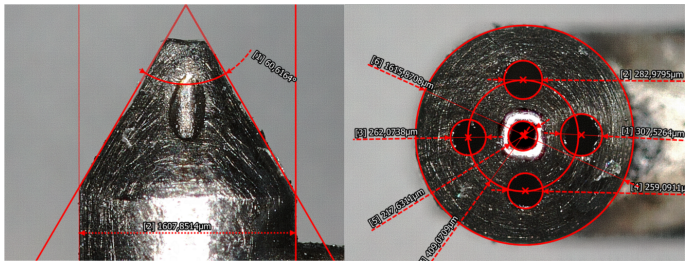

FIGURE 19. LEFT: CONE ANGLE OF 5HP-1, RIGHT: HOLE CIRCLE AND DIAMETER OF 5HP-1

larger yaw angles.

The manufacturers error for the cone angle of the four probe tips varies in a range of $\Delta\theta = 0.3°$. The accuracy of the position of the side holes is also in a tight range of $\Delta s = \pm 10\,\mu m$. Figure 19 shows the various measurement results for five-hole probe 1.

Figure 20 clearly shows the impact of particles in the flow on the surface of a five-hole probe even though a G2 filter was

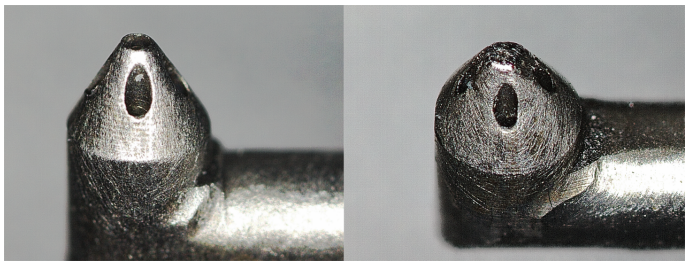

FIGURE 20. LEFT: UNUSED SPARE 5HP-4, RIGHT: 5HP-2 AFTER 300 TESTING HOURS

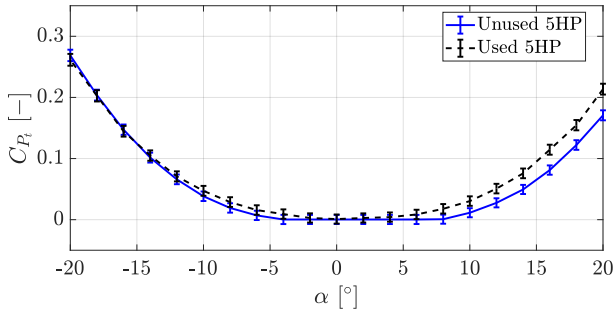

FIGURE 21. CHANGE OF TOTAL PRESSURE COEFFICIENT C_{P_t} OF 5HP-3 AFTER 300 TESTING HOURS DUE TO AGING

always installed at the inlet of the compressor rig. The increase in roughness and edge radii is clearly visible. Figure 21 is a plot of the total pressure coefficient C_{P_t} of 5HP-3 after around 300 test hours. A significant deviation is apparent, especially in the positive yaw angle direction. Hence, regular inspection, cleaning and recalibration of the probes is mandatory.

Influence of Reynolds Number

The variation in the Reynolds number applicable for the following investigations was defined as a multiple of the Reynolds number Re_1 that was set for the numerical calibration.
The Reynolds number was defined as:

$$Re_i = \frac{\rho_i \cdot v \cdot d_{Cyl}}{\eta} \tag{10}$$

To increase the Reynolds number, the reference pressure P_{ref} was multiplied by i:

$$\rho_i = \frac{i \cdot P_{ref}}{R_s \cdot T_s} \tag{11}$$

Table 3 describes the constants, which were held steady during the investigations.

TABLE 3. CONSTANT VALUES FOR RE VARIATION

v	104 $\frac{m}{s}$	$\boldsymbol{d}_{Cyl}$	1.59 *mm*
$\boldsymbol{\eta}$	$18.2 \cdot 10^{-6}$ *Pa* $\cdot$ *s*	$\boldsymbol{R}_s$	287.06 $\frac{J}{kg \cdot K}$
T	300 *K*	$\boldsymbol{P}_{ref}$	99432 *Pa*

TABLE 4. ACHIEVED REYNOLDS NUMBERS

i	0.5	1	2	3	6
$\boldsymbol{Re}_i[\cdot 10^4]$	0.525	1.05	2.1	3.15	6.3

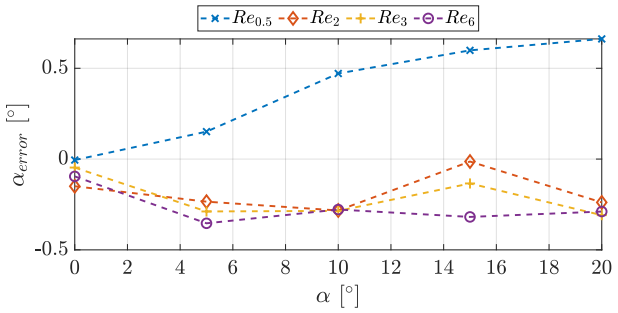

FIGURE 22. YAW ANGLE ERROR FOR DIFFERENT REYNOLDS NUMBERS

Increasing or decreasing the reference pressure P_{ref}, resulted in the Reynolds numbers tabulated in Tab. 4.

The numerical pressures $P_{PH1-PH5}$, measured at the measurement plane of the five holes for different Reynolds numbers Re_i and yaw angles α_k went through a standard data reduction routine using the original numerical calibration map, and the reduced yaw and pitch angles as well as total and static pressures were then compared to the actual angle setting of the probe within the domain and the pressure settings at the inlet, respectively.

To estimate the angle error $(\alpha,\beta)_{(error,i,k)}$, the actual set angle $(\alpha,\beta)_{(1,k)}$ of the probe is subtracted from the measured angle $(\alpha,\beta)_{(i,k,meas)}$. The yaw angle error α_{error} shows little dependency on Reynolds number across the incidence range α_k, when the Reynolds number is increased to values greater than the reference value Re_i (cf. Fig. 22). It varies within a corridor of $-0.4° < \alpha_{error} < 0°$. However, for the Reynolds number $Re_{0.5}$ which is less than the calibration Re_1, the error in yaw angle increases somewhat linearly with incidence up to 0.6°. Dominy et al. [8] also investigated this behavior in their experimental studies. For higher positive yaw angles and lower Reynolds numbers a separation bubble, triggered by the edge around PH1, was found to grow over PH4 thus reducing the measured pressure.

Figure 23 illustrates the error in the pitch angle β_{error} with

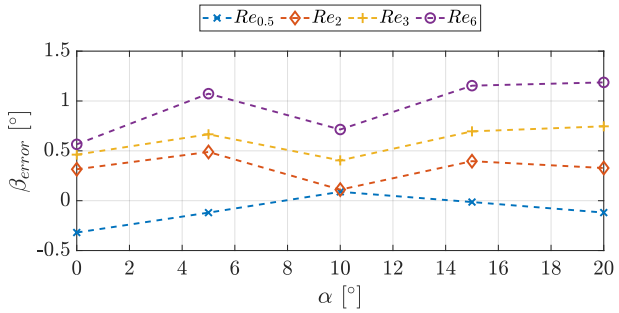

FIGURE 23. PITCH ANGLE ERROR FOR DIFFERENT REYNOLDS NUMBERS

respect to the Reynolds number Re_1 from the calibration. In contrast to the yaw angle, the lower $Re_{0.5}$ has no significant influence on the pitch angle measurement. However, the pitch angle error increases gradually as the Reynolds number increases while remaining largely insensitive to the incident angle α. This results primarily from the decreasing pressure at PH3 for higher Reynolds numbers. The same effect of a decreasing pressure coefficient with increasing Re was also observed by Passmann et al. [10]. In this case, the influence of the stem might cause the imbalance in the effect of Re between PH2 and PH3. The maximum error of 1.2° at $\alpha = 20°$ occurs at Re_6.

To estimate the total pressure error $P_{t,error}$, the numerically measured pressure $P_{t,meas}$ is compared to the total pressure P_t prescribed at the inlet:

$$P_{t,error,i,k} = \frac{P_{t,i,k,meas} - P_{t,i}}{P_{t,i}} \tag{12}$$

The error in the total pressure behaves in a qualitatively similar manner to the error in the yaw angle measurement (cf. Fig. 24). The maximum error at $Re_{0.5}$ and maximum incident angle α is about $\pm 0.06\%$, which is of the same order of magnitude as the accuracy of the pressure scanner used for the experiments.

Figure 25 is a plot of the error in the static pressure measurement $P_{s,error}$. The error is defined as:

$$P_{s,error,i,k} = \frac{P_{s,i,k,meas} - P_{s,i}}{P_{ref}} \tag{13}$$

The error in the static pressure is found to depend on the Reynolds number. With the maximum error approaching 0.2% it is greater than the total pressure error by a factor of > 3, a value that is no longer negligible.

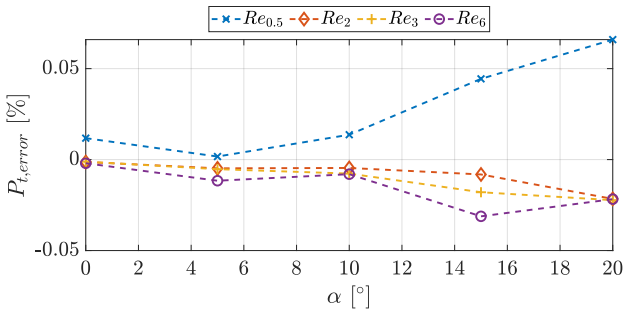

FIGURE 24. TOTAL PRESSURE ERROR FOR DIFFERENT REYNOLDS NUMBERS

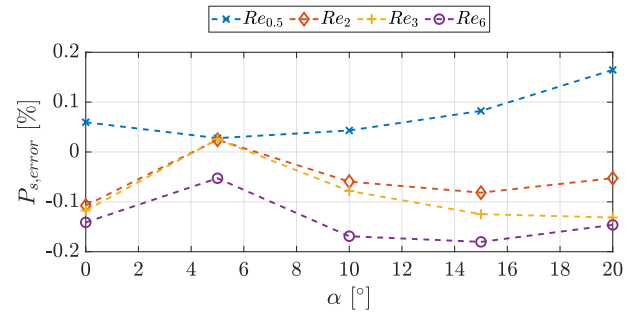

FIGURE 25. STATIC PRESSURE ERROR FOR DIFFERENT REYNOLDS NUMBERS

CONCLUSION AND OUTLOOK

A numerical model was set up using Ansys Fluent for a five-hole probe with a tip diameter of 1.59 mm and a cone angle of 60°. After an initial mesh resolution study, the numerical model was used to reproduce conditions equivalent to those of a calibration tunnel with a uniform low-turbulence flow and typical ambient conditions, at a Mach number of $Ma = 0.3$ and at varying yaw and pitch angles to obtain a numerical calibration map of the probe. The pressures inside the probe holes served as the convergence criteria. The results provide generally good agreement with the calibration data from the wind tunnel. Some differences are most probably caused by deviations between actual and nominal probe geometries, which could be observed under a microscope.

The analysis of the real probe geometry of a brand new probe in comparison to a significantly aged probe also reveals the impact of utilizing the probe in a compressor test rig with an inlet filter. The actual geometry changes significantly over time and therefore probes need to be periodically inspected, cleaned and recalibrated. This aging effect is reflected in the calibration coefficients.

The positive effect of modeling the probe holes has been discussed in detail. Measuring the pressure only over the surface of the probe cone leads to significant differences, a finding similar to the results obtained by LI et al. [7]. Even though the meshing becomes more complicated, the benefit appears to outweigh the added complexity.

To investigate the effect of Reynolds number on the probe characteristics, the probe Reynolds number was decreased by halving and increased by factors of two, three and six relative to the ambient conditions by decreasing or increasing the pressure at a given Mach number and simulations were then conducted while varying the yaw angle by up to 20°. The error in the total pressure measurement was found to be negligible with a maximum deviation of 0.06% relative to the actual total pressure. This insensitivity of the total pressure coefficient for small yaw angles was also observed during the experimental investigations conducted by Dominy et al. [8]. Passmann et al. [10] found the same behavior, although at even lower Re a noticeable change was discovered. The yaw angle error was also found to be generally small, only reaching 0.6° at maximum incidence for the smallest Reynolds number. A significant error could be observed for the pitch angle measurement which reaches 1.2° for the highest Reynolds number. The static pressure error was found to be small but not insignificant at up to 0.2%. Furthermore, the error with varying yaw angle tends to remain constant for most coefficients. Finally, the influence of the Reynolds number within the investigated range seems to be small but not completely negligible. How much the Reynolds number effect influences the measurement results also depends on the accuracy of the measurement equipment being used.

As it has been possible to demonstrate the accuracy of a numerical calibration, further investigations into pitch angle variations in combination with yaw angle variations at different Reynolds numbers are required. Also, surface scanning of actual probes using a computer tomograph is planned in order that the actual probe geometry can be numerically calibrated and the effect of geometry deviations on the numerical calibration and investigations can be minimized.

ACKNOWLEDGEMENTS

The authors gratefully thank Christian Aalburg from GE Aviation for his continuous great support and supervision and also Katya Menter from Ansys for her extremely helpful input.

This project has received funding from the Clean Sky 2 Joint Undertaking (JU) under grant agreement No *821435*. The JU receives support from the European Unions Horizon 2020 research and innovation programme and the Clean Sky 2 JU members other than the Union.

NOMENCLATURE

5HP	Five-hole probe
C	Non-dimensional calibration coefficient

d	Diameter
Ma	Mach number
P	Pressure
PH	Probe Hole
R	Radius
R_s	Specific gas constant
Re	Reynolds number
s	Distance
T	Temperature
v	Velocity
y^+	Dimensionless wall distance
x,y,z	Cartesian coordinates
Z	Value considering errors
$\overline{Z}$	Expected value

Greek Symbols

α	Yaw angle
β	Pitch angle
ε	Error
η	Dynamic viscosity
ρ	Density
Δ	Difference between two values
θ	Cone angle of 5HP

Subscribts

∞	Initial value
avg	Average equivalent value
Cyl	Cylinder
d	Dynamic value
exp	Experimental value
i	Factor
k	Yaw angle setting
max	Maximum equivalent value
meas	Measured (calculated by pressures)
num	Numerical value
ref	Reference value
s	Static value
t	Total value

REFERENCES

[1] de Guzman, M. M., Fletcher, C., and Hooper, J. D., 1994. "Computational Investigation of Cobra Probe Operation". *International Journal of Numerical Methods for Heat & Fluid Flow,* ***4***(5), pp. 425–445.

[2] Coldrick, S., Ivey, P. C., and Wells, R. G., 2004. "The Influence of Compressor Aerodynamics on Pressure Probes: Part 2 - Numerical Models". *Proceedings of the ASME Turbo Expo*, pp. 515–520.

[3] Aschenbruck, J., Hauptmann, T., and Seume, J. R., 2015. "Influence of a Multi-Hole Pressure Probe on the Flow Field in Axial-Turbines". *Proceedings of 11th European Conference on Turbomachinery Fluid Dynamics & Thermodynamics*.

[4] Passmann, M., aus der Wiesche, S., and Joos, F., 2019. "Numerical Calibration of 3D Printed Five-Hole Probes for the Transonic Flow Regime". *Proceedings of the ASME - JSME - KSME Joint Fluids Engineering Conference*.

[5] Sanders, C., Terstegen, M., Hölle, M., Jeschke, P., Schönenborn, H., and Fröbel, T., 2017. "Numerical Studies on the Intrusive Influence of a Five-Hole Pressure Probe in a High-Speed Axial Compressor". *ASME Turbo Expo*.

[6] Arguelles Diáz, K. M., Fernandez Oro, J. M., Blanco Marigorta, E., and Barrio Perotti, R., 2010. "A Numerical 3-D Model of a Trapezoidal Three-Hole Pneumatic Pressure Probe for Incompressible Flow". *Proceedings of the ASME Fluids Engineering Division Summer Conference*, pp. 159–167.

[7] LI, Y., and Bohn, D., 2000. "Numerical Investigation of the Influence of Reynolds Number on Probe Measurements". *Tsinghua Science and Technology,* ***5***, pp. 400–403.

[8] Dominy, R. G., and Hodson, H. P., 1993. "An Investigation of Factors Influencing the Calibration of Five-Hole Probes for Three-Dimensional Flow Measurements". *Journal of Turbomachinery,* ***115***(3), pp. 513–519.

[9] Lee, S. W., and Jun, S. B., 2005. "Reynolds Number Effects on the Non-Nulling Calibration of a Cone-Type Five-Hole Probe for Turbomachinery Applications". *Journal of Mechanical Science and Technology,* ***19***(8), pp. 1632–1648.

[10] Passmann, M., aus der Wiesche, S., Povey, T., and Bermann, D., 2020. "Effect of Reynolds Number on Five-Hole Probe Performance: Experimental Study of the Open-Access Oxford Probe". *Proceedings of the ASME Turbo Expo*.

[11] Treaster, A. L., and Yocum, A. M., 1978. "The Calibration and Application of Five-Hole Probes". *International Instrumentation Symposium*, pp. 255–266.

[12] Willinger, R., and Haselbacher, H., 2003. "A Three-Hole Pressure Probe Exposed to Velocity Gradient Effects - Experimental Calibration and Numerical Investigation". *The 12th International Conference on Fluid Flow Technologies*, pp. 413–420.

[13] Ansys, 2020. "Ansys Fluent Mosaic Technology Automatically Combines Disparate Meshes with Polyhedral Elements for Fast, Accurate Flow Resolution". *Ansys - White Paper*, November.

[14] Menter, F. R., Lechner, R., Ansys German GmbH, and Matyushenko, A., 2020. "Best Practice: Generalized k-omega Two-Equation Turbulence Model in Ansys CFD (GEKO)". *Ansys - Technical Report*.